



**HAL**  
open science

## Graphene Oxide Sheets Decorated with Octahedral Molybdenum Cluster Complexes for Enhanced Photoinactivation of *Staphylococcus aureus*

Régis Guégan, Xiaoxue Cheng, Xiang Huang, Zuzana Nemeckova, Michaela Kubáňová, Jaroslav Zelenka, Tomáš Ruml, Fabien Grasset, Yoshiyuki Sugahara, Kamil Lang, et al.

► **To cite this version:**

Régis Guégan, Xiaoxue Cheng, Xiang Huang, Zuzana Nemeckova, Michaela Kubáňová, et al.. Graphene Oxide Sheets Decorated with Octahedral Molybdenum Cluster Complexes for Enhanced Photoinactivation of *Staphylococcus aureus*. *Inorganic Chemistry*, 2023, 62 (35), pp.14243-14251. 10.1021/acs.inorgchem.3c01502 . hal-04196513

**HAL Id: hal-04196513**

**<https://hal.science/hal-04196513>**

Submitted on 26 Oct 2023

**HAL** is a multi-disciplinary open access archive for the deposit and dissemination of scientific research documents, whether they are published or not. The documents may come from teaching and research institutions in France or abroad, or from public or private research centers.

L'archive ouverte pluridisciplinaire **HAL**, est destinée au dépôt et à la diffusion de documents scientifiques de niveau recherche, publiés ou non, émanant des établissements d'enseignement et de recherche français ou étrangers, des laboratoires publics ou privés.



Distributed under a Creative Commons Attribution 4.0 International License

This document is confidential and is proprietary to the American Chemical Society and its authors. Do not copy or disclose without written permission. If you have received this item in error, notify the sender and delete all copies.

**Graphene oxide sheets decorated with octahedral molybdenum cluster complexes for enhanced photoinactivation of *Staphylococcus aureus***

Journal:	<i>Inorganic Chemistry</i>
Manuscript ID	ic-2023-015028.R2
Manuscript Type:	Article
Date Submitted by the Author:	01-Aug-2023
Complete List of Authors:	Guegan, Regis; Waseda University; Interfaces Confinement Matériaux et Nanostructures Cheng, Xiaoxue; Waseda University Faculty of Science and Engineering Huang, Xiang; Waseda University Faculty of Science and Engineering Nemeckova, Zuzana; Ustav anorganické chemie Akademie ved Ceske republiky, Materials Chemistry Kubanová, Michaela; University of Chemistry and Technology Prague Department of Biochemistry and Microbiology Zelenka, Jaroslav; Vysoka skola chemicko-technologicka v Praze, Department of Biochemistry and Microbiology Ruml, Tomáš; Vysoka skola chemicko-technologicka v Praze, Dpt. of Biochemistry and Microbiology Grasset, Fabien; CNRS, UMI3629; ISCR Sugahara, Yoshiyuki ; Waseda University Faculty of Science and Engineering Lang, Kamil; Institute of Inorganic Chemistry of the Czech Academy of Sciences, Kirakci, Kaplan; Akademie Ved Ceske Republiky Ustav anorganické chemie,

SCHOLARONE™  
Manuscripts

1  
2  
3 **Graphene oxide sheets decorated with octahedral molybdenum cluster complexes for**  
4 **enhanced photoinactivation of *Staphylococcus aureus***  
5  
6  
7

8 Régis Guégan<sup>1,2\*</sup>, Xiaoxue Cheng<sup>3</sup>, Xiang Huang<sup>3</sup>, Zuzana Němečková,<sup>4</sup> Michaela  
9 Kubanová<sup>5</sup>, Jaroslav Zelenka<sup>5</sup>, Tomas Ruml<sup>5</sup>, Fabien Grasset<sup>6,7</sup>, Yoshiyuki Sugahara<sup>3,8</sup>,  
10 Kamil Lang<sup>4</sup>, Kaplan Kirakci<sup>4\*</sup>  
11  
12

13 <sup>1</sup>*Global Center for Science and Engineering, Waseda University, 3-4-1 Okubo, Shinjuku-ku,*  
14 *Tokyo 169-8555, Japan*  
15

16 <sup>2</sup>*Interfaces, Confinement, Matériaux et Nanostructures ICMN-UMR 737, CNRS-Université*  
17 *d'Orléans, 1 Rue de la Férollerie, 45100 Orléans, France*  
18

19 <sup>3</sup>*Department of Applied Chemistry, Waseda University, Faculty of Science and Engineering,*  
20 *3-4-1 Okubo, Shinjuku-ku, Tokyo 169-8555, Japan*  
21

22 <sup>4</sup>*Institute of Inorganic Chemistry of the Czech Academy of Sciences, 250 68 Husinec-Řež,*  
23 *Czech Republic*  
24

25 <sup>5</sup>*Department of Biochemistry and Microbiology, University of Chemistry and Technology*  
26 *Prague, 166 28 Praha, Czech Republic*  
27

28 <sup>6</sup>*Institut des Sciences Chimiques de Rennes, ISC-UMR 6226, CNRS-Université de Rennes 1,*  
29 *263 avenue du Général Leclerc, 35700 Rennes, France*  
30

31 <sup>7</sup>*CNRS–Saint-Gobain–NIMS, IRL3629, Laboratory for Innovative Key Materials and*  
32 *Structures (LINK), National Institute for Materials Science, 1-1 Namiki, Tsukuba 305-0044,*  
33 *Japan*  
34

35 <sup>8</sup>*Kagami Memorial Institute for Materials Science and Technology, Waseda University, 2-8-*  
36 *26 Nishiwaseda, Shinjuku-ku, Tokyo 169-0051, Japan*  
37  
38

39 *\*email: regis.guegan@univ-orleans.fr, kaplan@iic.cas.cz*  
40  
41  
42

43 **Abstract**  
44

45 The emergence of multidrug-resistant microbial pathogens poses a significant threat,  
46 severely limiting the options for effective antibiotic therapy. This challenge can be overcome  
47 through the photoinactivation of pathogenic bacteria using materials generating reactive  
48 oxygen species upon exposure to visible light. These species target vital components of living  
49 cells, significantly reducing the likelihood of resistance development by the targeted pathogens.  
50 In our research, we have developed a nanocomposite material consisting of an aqueous  
51 colloidal suspension of graphene oxide sheets adorned with nanoaggregates of octahedral  
52 molybdenum cluster complexes. The negative charge of the graphene oxide and the positive  
53 charge of the nanoaggregates promoted their electrostatic interaction in aqueous medium, and  
54  
55  
56  
57  
58  
59  
60

1  
2  
3 close cohesion between the colloids. Upon illumination with blue light, the colloidal system  
4 exerted a potent antibacterial effect against planktonic cultures of *Staphylococcus aureus*  
5 largely surpassing the individual contributions of the components. The underlying mechanism  
6 behind this phenomenon lies in the photoinduced electron transfer from the nanoaggregates of  
7 the cluster complexes to the graphene oxide sheets, which triggers the generation of reactive  
8 oxygen species. Thus, leveraging the unique properties of graphene oxide and light-harvesting  
9 octahedral molybdenum cluster complexes can open more effective and resilient antibacterial  
10 strategies.  
11  
12  
13  
14  
15  
16  
17  
18

19 **Keywords:** photosensitizer, bactericide properties, graphene oxide, molybdenum cluster,  
20 nanocomposite, bacteria  
21  
22  
23

## 24 **Introduction**

25  
26 Microbial pathogens exhibiting multidrug-resistance constitute a serious hazard,  
27 especially to cancer and immunocompromised patients, and restricts the choices for adequate  
28 antibiotic therapy.<sup>1,2</sup> Among the many possible ways to inactivate pathogens, their  
29 photoinactivation by materials able to produce reactive oxygen species (ROS) upon visible-  
30 light irradiation represents an elegant way to achieve this goal, as ROS attack several critical  
31 components of living cells thus limiting the emergence of resistance to the treatment.  
32  
33  
34

35  
36 In this respect, octahedral molybdenum cluster complexes are efficient singlet oxygen  
37 photosensitizers and have recently demonstrated major potential as molecular antibacterial  
38 agents or for the design of light-triggered disinfecting surfaces.<sup>3,4,5,6,7,8,9</sup> These clusters are  
39 stabilized by eight inner ligands, usually iodine atoms and six labile apical ligands of inorganic  
40 or organic nature. Upon excitation from the UV up to the green light, the resulting complexes  
41 exhibit long lived triplet states that relax via a red-NIR phosphorescence or by energy transfer  
42 to molecular oxygen to form the highly reactive singlet oxygen  $O_2(^1\Delta_g)$ .<sup>10,11,12</sup> Several studies  
43 have reported the effect of these complexes for the photoinactivation of planktonic cultures and  
44 biofilms of both gram-negative and gram-positive bacteria.<sup>3,4,5,6,7,8,9</sup> When compared to organic  
45 photosensitisers, these cluster complexes are less prone to self-quenching of their luminescent  
46 properties due to aggregation at high concentration or photobleaching which can limit the  
47 efficiency and robustness of their derived materials.<sup>7</sup>  
48  
49  
50  
51  
52  
53  
54  
55  
56

57 Graphene oxide (GO) sheets, prepared from the etching and oxidation of graphite,  
58 exhibit outstanding properties: large specific surface area, electrical and mechanical properties,  
59  
60

1  
2  
3 that tackle the interests of both the scientific and industrial communities.<sup>13,14,15,16,17</sup> While the  
4 inclusion of oxygen atoms within carbon sheets modulates their electrical properties, it also  
5 confers a hydrophilic behaviour to GO, making them dispersible in aqueous media as a  
6 supporting phase for, e.g., complexes or nanoparticles to prepare nanocomposite  
7 materials.<sup>18,19,20,21,22</sup> In addition to the hydrophilic moieties, GO display unaltered hydrophobic  
8 graphene like patches which represent many reaction/adsorption sites for the association with  
9 other colloids. As in the case of other carbon-based nanomaterials (carbon nanotubes, etc.), GO  
10 sheets exhibit antibacterial properties, of which origin comes from the physical presence of the  
11 sheets as well as their chemical activities.<sup>13,16,17</sup> Indeed, it has been recognized that GO sheets  
12 wrap around bacteria causing irreversible physical damage to the cell membranes while  
13 chemically increasing the cellular oxidative stress leading to the end of the bacterial  
14 development.<sup>13</sup>

15  
16  
17  
18  
19  
20  
21  
22  
23  
24 The association of photosensitizing organic compounds such as hypocrellin A to GO  
25 sheets lead to nanocomposites showing long-time effects for eradication of cancer cells.<sup>23</sup> In  
26 this case, GO sheets act as a preservation matrix for hypocrellin A that could generate  $O_2(^1\Delta_g)$   
27 on a long-time scale. In another study, the association of porphyrins with GO imparts the  
28 nanocomposites with antibacterial properties.<sup>24</sup> The mechanism behind the antibacterial  
29 activity was assigned to fast electron transfer from the excited singlet states of porphyrin to the  
30 conduction band of GO resulting in the production of ROS by the sheets.<sup>24</sup> Thus, we surmise  
31 that the association of such cluster complexes with GO could lead to enhancement of  
32 photoinactivation of bacteria. In fact, various composites of these cluster complexes with GO  
33 have already been utilized with promising results for applications such as photocatalytic water  
34 reduction, photodegradation of organics, or gas sensing, but so far, no such composite material  
35 has been studied for its antibacterial properties.<sup>25,26,27,28,29</sup>

36  
37  
38  
39  
40  
41  
42  
43  
44  
45 This research work describes the association of the cluster compound,  
46  $[Mo_6I_8(OCOC_4H_8PPh_3)_6]Br_4$  (**Mo<sub>6</sub>**), with GO sheets (Fig. 1) for the preparation of  
47 nanocomposites with antibacterial properties. Dispersed in dimethyl sulfoxide to provide a  
48 homogeneous dispersion of the components and long-term durability of Mo<sub>6</sub> complexes, and  
49 then added to aqueous medium, GO sheets act as a template or supporting phase of Mo<sub>6</sub> in the  
50 form of nanoaggregates interacting mainly via electrostatic forces. After a careful  
51 characterization of the morphology, cohesion, and structure of the nanocomposites as well as  
52 of their photophysical properties by various complementary techniques, their bactericide  
53  
54  
55  
56  
57  
58  
59  
60

properties against *Staphylococcus aureus* are demonstrated through a comparative study of the efficiency of the whole individual materials.

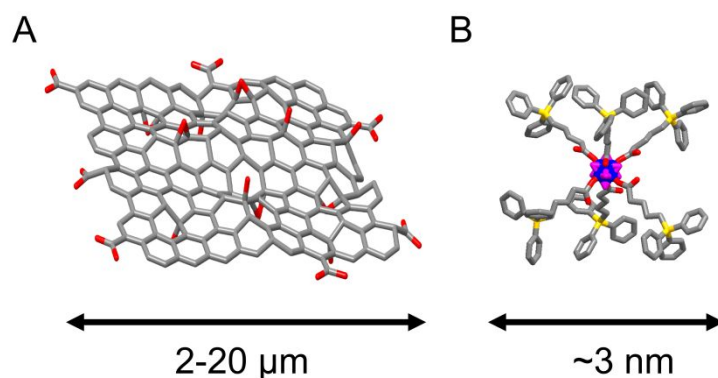


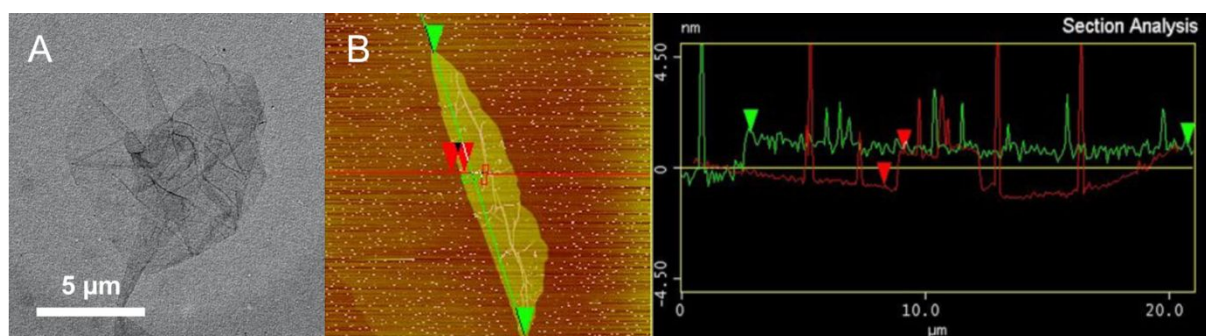
**Figure 1.** Schematic representation of (A) GO sheets and (B) positively charged Mo<sub>6</sub> complex [Mo<sub>6</sub>I<sub>8</sub>(OCOC<sub>4</sub>H<sub>8</sub>PPh<sub>3</sub>)<sub>6</sub>]<sup>4+</sup>. Color codes: carbon (grey), oxygen (red), phosphorus (yellow), molybdenum (blue), iodine (magenta).

## Results and discussion

### *Preparation and characterization of GO*

GO sheets were prepared using the modified Hummer's method based on oxidation and exfoliation of graphite.<sup>30</sup> As demonstrated by several studies, the diversity of the chemical landscape of GO sheets and their 2D-surfactant character (Pickering emulsion) allow for dispersion in many polar and non-polar organic solvents.<sup>14,31</sup> However, the use of dimethyl sulfoxide (DMSO), a polar solvent often used in biological experiments, failed so far to give stable GO dispersions.<sup>31</sup> In the aforementioned study, the sheets were dried in a vacuum oven which favoured the re-stacking of the sheets into the initial graphite-like layered structure, slowing down their subsequent exfoliation and leading to the formation of GO agglomerates and sedimentation of the graphite oxide. In the present study, the prepared GO sheets, displaying a similar oxidation rate, were lyophilized which allowed for an easy dispersion in DMSO and water at a concentration of 1 mg mL<sup>-1</sup>, higher than that previously tested using a wide range of solvents (0.5 mg mL<sup>-1</sup>) (Fig. S1 in the Supporting Information).<sup>31</sup> This feature was confirmed by transmission electron microscopy (TEM) and atomic force microscopy (AFM) observations, indicating the absence of re-stacking and aggregation of the sheets as the images showed a majority of individual sheets with a lateral size in the 2-20 μm range and a

1  
2  
3 thickness close to 1 nm (Figs. 2 and S2 in the Supporting Information), an important point to  
4 consider for future applications based on single carbon nanomaterials.  
5  
6  
7



8  
9  
10  
11  
12  
13  
14  
15  
16  
17  
18  
19 **Figure 2.** Characterization of the GO sheets by TEM (A) and AFM with the corresponding  
20 section analysis (B).  
21  
22  
23

24  
25 The GO sheets, after being dispersed in water or DMSO, were collected and  
26 characterized by Raman scattering and XPS spectroscopy (Fig. 3), to assess the possible  
27 chemical changes after their immersion in DMSO. As expected, the Raman spectra of the GO  
28 showed two characteristic bands of graphitized materials, i.e., the D band reflecting structural  
29 defects due to inclusion of oxygen atoms in the carbon structure or holes, and the G band  
30 representative of the original graphite organization.<sup>32</sup> The intensity ratio  $I_D/I_G$  is an indicator of  
31 the degree of graphitization of the GO sheets and remained the same for the GO sheets (0.87)  
32 before and after immersion in water or DMSO (Table 1). It underlines the absence of any  
33 modification, nor physical structural alteration of the sheets after the freeze-drying operation.  
34 However, the XPS spectrum of the DMSO immersed GO seemed to display a higher proportion  
35 of C=O double bonds at the expense of a lowering of C-C bonds (graphite areas), which is  
36 contradictory with the Raman data that suggested the same proportion of graphitic domains.  
37 Since DMSO is a rather viscous solvent with a high boiling point, it is likely that some DMSO  
38 molecules remain on the surface of the GO sheets and the C-S band could overlap with the C  
39 1s spectrum of the GO as well as the resulting distribution of the various bonds. Nevertheless,  
40 the characterization by Raman scattering clearly evidences that the GO sheets were not altered  
41 neither physically nor chemically after their lyophilization and dispersion in DMSO.  
42  
43  
44  
45  
46  
47  
48  
49  
50  
51  
52  
53  
54  
55  
56  
57  
58  
59  
60

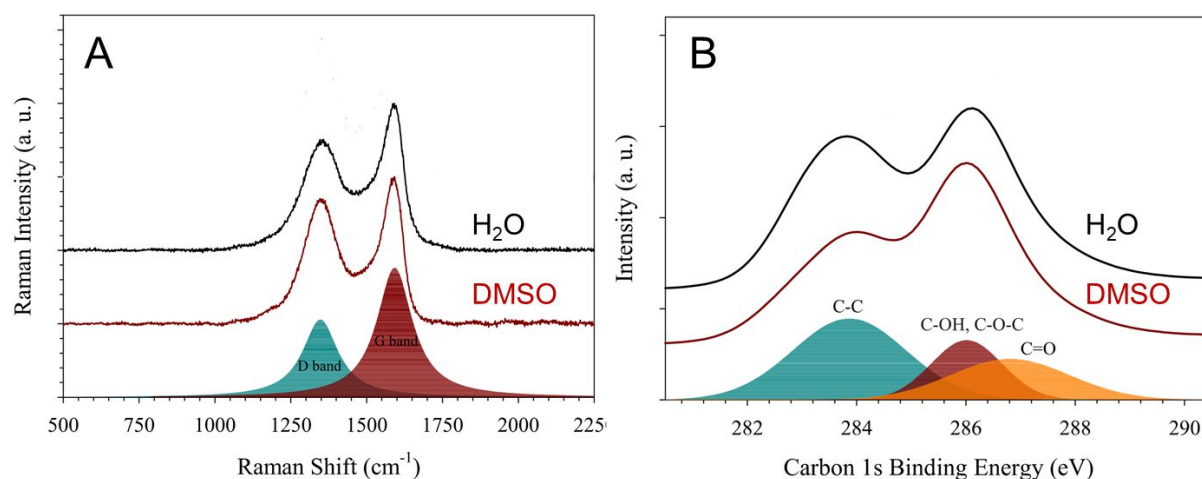


**Figure 3.** Raman scattering (A) and XPS (B) of the GO sheets after being dispersed in water (black) and in DMSO (red).

**Table 1.** Component area percentages of the GO sheets dispersed in H<sub>2</sub>O and DMSO and corresponding ratios of the G band over the D band.

Sample	C-C	C-OC, C-OH	C=O	$I_D/I_G$ (Raman)
GO (H <sub>2</sub> O)	50.2%	42.6%	7.2%	0.87
GO (DMSO)	44.6%	32.8%	22.6%	0.87

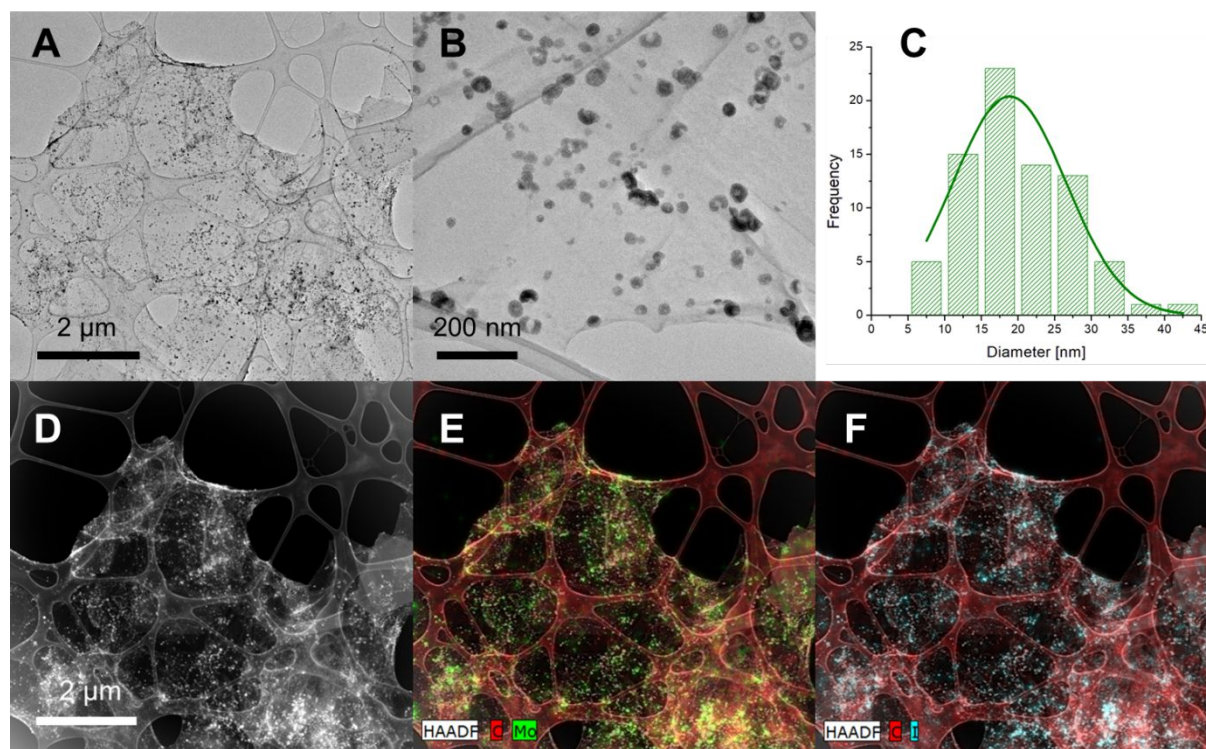
#### Preparation and characterization of GO/Mo<sub>6</sub> nanocomposites

The dispersibility of the GO sheets in DMSO after a freeze-drying operation, with the formation of stable dispersions, opens new routes for the preparation of nanocomposites. Leaning against this strategy, the nanocomposites were prepared by mixing the lyophilized GO and [Mo<sub>6</sub>I<sub>8</sub>(OCOC<sub>4</sub>H<sub>8</sub>PPh<sub>3</sub>)<sub>6</sub>]Br<sub>4</sub> in DMSO for 24 hours under magnetic stirring. Mo<sub>6</sub> complex suffers from a lack of stability and poor solubility in aqueous media where its apical ligands are replaced within days, but it is well soluble in DMSO where the hydrolytic process is greatly slowed down.<sup>3</sup> Thus, DMSO solutions of Mo<sub>6</sub> complex did not exhibit any significant aggregation by showing an average size of  $3.1 \pm 1$  nm (Z-average = 6.0 nm, PDI = 0.20) (Fig. S3 in the Supporting Information), which is consistent to the size of isolated Mo<sub>6</sub> complex. Due to the targeted antibacterial application, the GO/Mo<sub>6</sub> nanocomposite was studied in the form of an aqueous colloidal dispersion which was obtained by adding the aliquots of the DMSO dispersion (1 mg mL<sup>-1</sup>) to deionized water (DMSO/H<sub>2</sub>O, 1 % v/v).

1  
2  
3 Transmission electron microscopy of a drop of the resulting aqueous dispersion of GO/Mo<sub>6</sub>  
4 deposited on a TEM grid documented GO sheets decorated by nanoaggregates with an average  
5 size of  $19 \pm 8$  nm and made of Mo<sub>6</sub> as demonstrated by the HAADF elemental mapping of Mo  
6 and I, (Figs. 4, S4 in the Supporting Information). The Mo<sub>6</sub> nanoaggregates immobilized on  
7 the surface of GO are apparently formed during the addition of the DMSO dispersion to H<sub>2</sub>O.  
8 Indeed, dynamic light scattering of pure Mo<sub>6</sub> in water evidenced nanoaggregates with an  
9 average size by number of  $31 \pm 10$  nm (*Z*-average = 110 nm, PDI = 0.37) (Fig. S3 in the  
10 Supporting Information), reminiscent of the nanoparticles of other pure cluster compounds  
11 obtained via the solvent displacement method.<sup>33,34,35</sup> X-ray powder diffraction pattern of  
12 GO/Mo<sub>6</sub> featured a very broad peak at approximately 7° demonstrating the amorphous  
13 character of the nanocomposite material (Figure S5 in the Supporting Information). ICP-MS  
14 analysis of dried GO/Mo<sub>6</sub>, isolated by centrifugation of the water dispersion, revealed a  
15 molybdenum content of 68.1 mg g<sup>-1</sup> slightly lower than the theoretical content of 70.5 mg g<sup>-1</sup>,  
16 indicating that the majority of the nanoaggregates of Mo<sub>6</sub> are immobilized at the surface of  
17 GO. This feature is in agreement with the absorption spectra of the supernatant after  
18 centrifugation of the GO/Mo<sub>6</sub> water dispersion, which evidenced only minute amount of free  
19 Mo<sub>6</sub> (Fig. S6 in the Supporting Information). The zeta potentials of the aqueous dispersions of  
20 GO and Mo<sub>6</sub> amounted to  $-34 \pm 13$  and  $8 \pm 6$  mV, respectively, in accordance with the  
21 ionization of the hydroxyl and carboxylic groups of GO and the presence of positive charges  
22 endowed by the apical ligands of Mo<sub>6</sub> at the surface of the nanoaggregates (Fig. S7 in the  
23 Supporting Information). The aqueous dispersion of GO/Mo<sub>6</sub> displayed a negative zeta  
24 potential of  $-19 \pm 8$  mV and the zeta potential distribution was characterized by a single peak  
25 located in the negative range of the zeta potential values. In accordance with the above-  
26 mentioned characterizations, these results confirm that, in aqueous medium, the majority of the  
27 positively charged Mo<sub>6</sub> nanoaggregates is immobilized at the GO surface, where they partially  
28 compensate for its negative charge.

29  
30  
31  
32  
33  
34  
35  
36  
37  
38  
39  
40  
41  
42  
43  
44  
45  
46  
47  
48  
49  
50  
51  
52  
53  
54  
55  
56  
57  
58  
59  
60  
Despite the mild conditions used for the preparation of the nanocomposite in DMSO and the  
bulkiness of the apical ligands making them poorly labile, it is still possible that an apical ligand  
exchange could occur in this solvent resulting in bonding of cluster complexes to the surface  
of GO. In this case, we should expect a homogeneous coverage of the GO surface by Mo<sub>6</sub>  
considering the high degree of structural defects due to inclusion of oxygen atoms evidenced  
by Raman spectroscopy. However, TEM images of the nanocomposite clearly show the non-  
continuous distribution of nanoaggregates of Mo<sub>6</sub> at the surface of GO (Figs. 4 and S4). Thus,  
the mechanism of the formation of the GO/Mo<sub>6</sub> nanocomposite can be tentatively ascribed to

1  
2  
3 the precipitation of positively charged nanoaggregates of hydrophobic Mo<sub>6</sub> after mixing the  
4 DMSO dispersions of GO and Mo<sub>6</sub> in water, followed by the immobilization of the  
5 nanoaggregates at the surface of GO mainly via electrostatic interactions. Indeed, it is unlikely  
6 that a significant ligand exchange with hydroxyl or carboxylates function of the GO could  
7 occur during the short period (minutes to hours) between the transfer of the DMSO dispersion  
8 to water and the measurement of the nanocomposite characteristics.  
9  
10  
11  
12  
13  
14



15  
16  
17  
18  
19  
20  
21  
22  
23  
24  
25  
26  
27  
28  
29  
30  
31  
32  
33  
34  
35  
36  
37  
38  
39  
40  
41  
42  
43  
44  
45  
46  
47  
48  
49  
50  
51  
52  
53  
54  
55  
56  
57  
58  
59  
60  
**Figure 4.** TEM images of GO/Mo<sub>6</sub> in the bright field (A, B) with the corresponding particle size distribution of Mo<sub>6</sub> nanoaggregates (C), and in the dark field (D) with the C, Mo (E) and C, I (F) HAADF elemental mapping.

The luminescence of Mo<sub>6</sub> complexes is influenced by their ligands as well as their immediate environment and can be taken as a sensitive indicator of the extent of interaction between Mo<sub>6</sub> and GO. Therefore, the photophysical properties of water dispersions of the nanocomposites and their individual components, freshly prepared in the same way as for DLS experiments, were investigated and are summarized in Table 2. The absorption spectrum of GO/Mo<sub>6</sub> was essentially a composite of its individual components GO and Mo<sub>6</sub> showing typical absorption bands of Mo<sub>6</sub> complexes in the UV/blue region and the featureless UV-vis absorption of GO extending to the red region (Fig. S8 in the Supporting Information). When

1  
2  
3 compared to free Mo<sub>6</sub> complex, the luminescence band of GO/Mo<sub>6</sub> was broader and the  
4 maximum was red-shifted from 706 nm for Mo<sub>6</sub> to approximately 722 nm for GO/Mo<sub>6</sub> (Fig.  
5 5A). A drastic decrease in the luminescence intensity was also noticed, as also evidenced by a  
6 significant drop of luminescence quantum yields from 0.24 for Mo<sub>6</sub> to 0.01 for GO/Mo<sub>6</sub>.  
7 Similarly, the average luminescence lifetime in argon-saturated dispersions decreased from 88  
8 μs for Mo<sub>6</sub> to 2.4 μs for GO/Mo<sub>6</sub> (Fig. 5B). It is worth noting that as-prepared DMSO  
9 dispersions of Mo<sub>6</sub> and GO/Mo<sub>6</sub> displayed comparable luminescence spectra indicating that  
10 the cluster complex was chemically unchanged prior to addition to aqueous medium as  
11 hydrolysis would be characterized by a red-shift of the emission maximum (Fig. S9 in the  
12 Supporting Information). In addition, the kinetics of hydrolysis of Mo<sub>6</sub> in aqueous medium  
13 were already reported showing that the wide majority of the cluster complexes remained intact  
14 after 24 h.<sup>3</sup> Thus, hydrolysis of Mo<sub>6</sub> complex in DMSO or immediately after addition to  
15 aqueous medium was excluded to account for the strong decrease in emission quantum yield  
16 and lifetime of GO/Mo<sub>6</sub> in water relative to pure Mo<sub>6</sub>. Instead, the presented results point out  
17 at electronic interactions between the immobilized nanoaggregates of Mo<sub>6</sub> and GO, leading to  
18 the quenching of their excited states.  
19  
20  
21  
22  
23  
24  
25  
26  
27  
28  
29  
30  
31  
32

33 **Table 2.** Photophysical parameters of water dispersions of GO, Mo<sub>6</sub>, and GO/Mo<sub>6</sub> at room  
34 temperature.<sup>a</sup>

36 <b>Sample</b>	37 $\lambda_L$ / nm	38 $\tau_T$ / μs	39 $\tau_{air}$ / μs	40 $\Phi_L$
41 <b>GO</b>	42 670	43 0.7 ns <sup>b</sup>	44 0.7 ns <sup>b</sup>	45 <0.01
46 <b>Mo<sub>6</sub></b>	47 706	48 88 <sup>b</sup>	49 29 <sup>b</sup>	50 0.24
51 <b>GO/Mo<sub>6</sub></b>	52 722	53 2.4 <sup>b</sup>	54 2.3 <sup>b</sup>	55 0.01

56 <sup>a</sup>  $\lambda_L$  is the maximum of luminescence emission bands (excited at 400 nm);  $\tau_T$  and  $\tau_{air}$  are the  
57 average luminescence lifetimes in argon- (oxygen-free) and air-saturated water, respectively  
58 (recorded at 700 nm, excited at 405 nm);  $\Phi_L$  is the luminescence quantum yield in argon-  
59 saturated solutions (excitation at 400 nm, experimental error of  $\Phi_L$  is  $\pm 0.01$ ); <sup>b</sup> The amplitude  
60 average lifetimes obtained by the biexponential analysis of corresponding kinetic curves.

61 Contrasting with free Mo<sub>6</sub> nanoaggregates (Fig. S10 in the Supporting Information),  
62 there was negligible quenching of the triplet states by oxygen after their deposition onto the  
63 GO sheets as evidenced by the average luminescence lifetimes of GO/Mo<sub>6</sub> in air- and argon-  
64 saturated water (2.4 and 2.3 μs, respectively, Table 2) (Fig. 5C). This result also indicates fast

competitive quenching of the triplet states of deposited Mo<sub>6</sub>, probably associated with photoinduced electron transfer between Mo<sub>6</sub> and the GO sheets and suggest a poor production of O<sub>2</sub>(<sup>1</sup>Δ<sub>g</sub>) by deposited Mo<sub>6</sub> upon irradiation. Note that a very weak red emission from a GO water dispersion was observed when exciting at 400 nm. It was characterized by a broad band with a maximum at approximately 670 nm and an emission lifetime of 0.7 ns, which is consistent with the reports on GO (Table 2, Fig. S11 in the Supporting Information).<sup>16</sup>

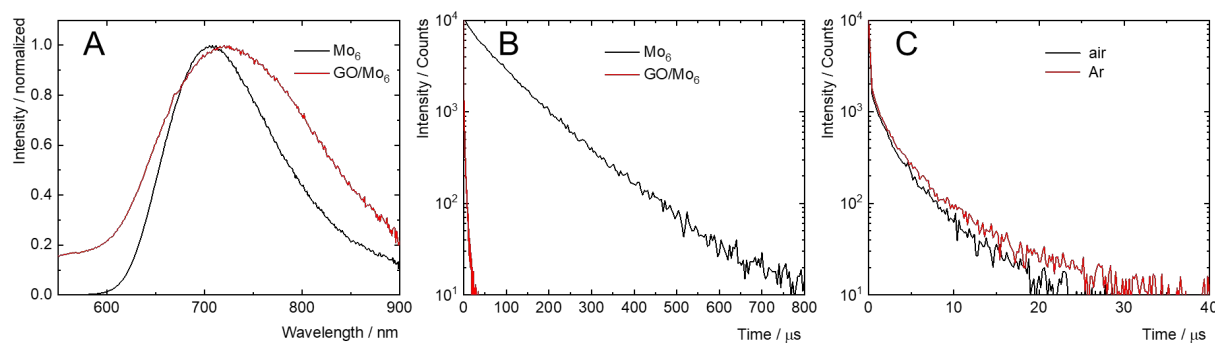


**Figure 5.** (A) Normalized luminescence spectra of Mo<sub>6</sub> (black) and GO/Mo<sub>6</sub> (red) in argon-saturated water, excitation was at 400 nm. (B) Luminescence decay kinetics of Mo<sub>6</sub> (black) and GO/Mo<sub>6</sub> (red) in argon-saturated water. Excitation was at 405 nm and emission at 700 nm. (C) Luminescence decay kinetics of GO/Mo<sub>6</sub> in air- (black) and argon- (red) saturated water dispersions. Excitation was at 405 nm and emission at 700 nm.

The inhibition of O<sub>2</sub>(<sup>1</sup>Δ<sub>g</sub>) production by deposited nanoaggregates of Mo<sub>6</sub> in GO/Mo<sub>6</sub> was confirmed by measuring the weak phosphorescent signal of O<sub>2</sub>(<sup>1</sup>Δ<sub>g</sub>) centred at approximately 1270 nm. Indeed, while Mo<sub>6</sub> showed a typical phosphorescence band of O<sub>2</sub>(<sup>1</sup>Δ<sub>g</sub>), as previously reported for this complex,<sup>3</sup> both GO and GO/Mo<sub>6</sub> did not display any detectable signal in the same spectral region confirming that GO and GO/Mo<sub>6</sub> did not produce appreciable amount of O<sub>2</sub>(<sup>1</sup>Δ<sub>g</sub>) under these conditions, as previously reported for GO (Fig. 6A).<sup>36</sup> In order to evaluate the capacity of the nanocomposite to generate other reactive oxygen species, such as superoxide, hydrogen peroxide, or hydroxyl radical, we employed an oxidation probe, namely 2',7'-dichlorofluorescein diacetate (DCF-DA). It is a chemically reduced form of fluorescein commonly used as an indicator for ROS. DCF-DA was added to water dispersions containing various concentrations of GO/Mo<sub>6</sub> (0, 0.25, 0.5, 1 and 2 w/w%) followed by irradiation with 460 nm light. The probe was oxidized thus becoming fluorescent, and the amount of oxidation was dose- and time-dependent evidencing the capacity of GO/Mo<sub>6</sub> to photogenerate reactive oxygen species (Fig. 6B).

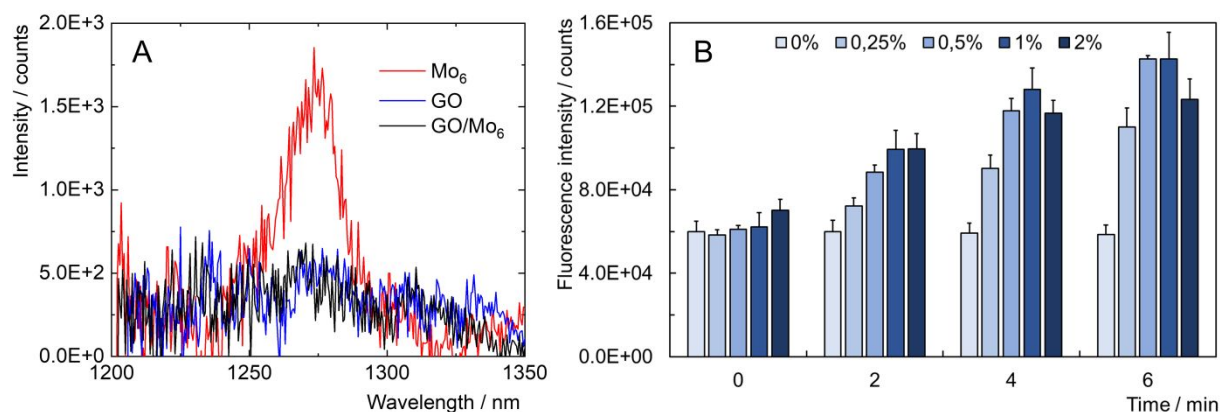


**Figure 6.** (A) Singlet oxygen phosphorescence band of Mo<sub>6</sub> (red), GO (blue) and GO/Mo<sub>6</sub> (black) in oxygen-saturated water. (B) Evaluation of the oxidation of the DCF-DA probe by various concentrations of GO/Mo<sub>6</sub> in water (0, 0.25, 0.5, 1, 2 %) under various blue-light irradiation time (460 nm). Bars labelled 0 % are control experiments in the absence of GO/Mo<sub>6</sub>.

Overall, the observed changes in the zeta potentials and luminescence parameters when comparing Mo<sub>6</sub> and GO/Mo<sub>6</sub> point out at strong electrostatic interactions between the GO sheets and the nanoaggregates of Mo<sub>6</sub> in aqueous medium. The quenching of the luminescence of Mo<sub>6</sub> by GO inhibits the formation of O<sub>2</sub>(<sup>1</sup>Δ<sub>g</sub>). This feature appears to be related to a photoinduced electron transfer from the excited states of the Mo<sub>6</sub> complex to the conduction band of GO and leads to the formation of ROS, probably superoxide, hydrogen peroxide, or hydroxyl radical, as previously reported in the literature.<sup>37,38,39</sup>

#### *Bactericide properties of the GO/Mo<sub>6</sub> nanocomposites*

The photoinactivation properties of GO/Mo<sub>6</sub> and its individual components were evaluated against planktonic culture of *S. aureus*, a Gram-positive spherically shaped bacterium. Despite acting as a commensal of the human microbiota, it can be the cause of skin and respiratory infections as well as food poisoning. *S. aureus* constitutes one of the leading lethal pathogens and is associated with antimicrobial resistance, making it an ideal target for photodynamic inactivation.<sup>1,2</sup> The cultures of *S. aureus* were incubated as planktonic cells with GO, Mo<sub>6</sub> and GO/Mo<sub>6</sub> dispersions and illuminated with 460 nm light.

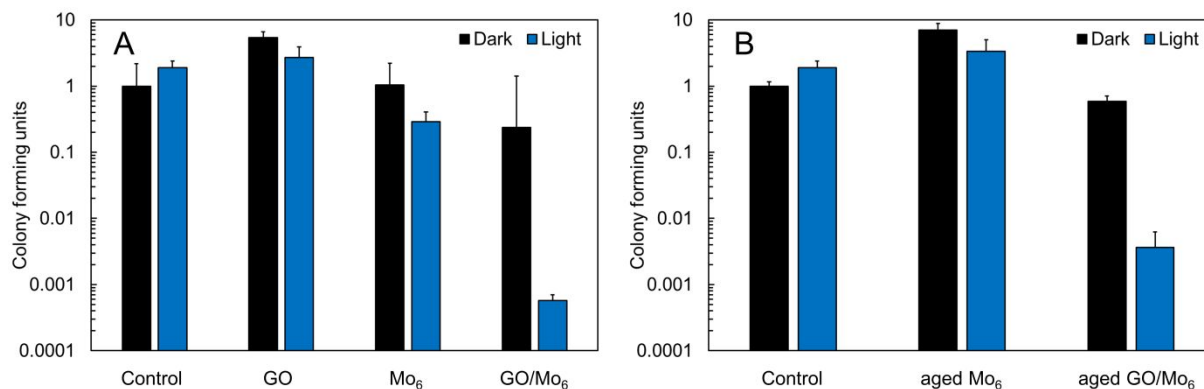


**Figure 7.** Photoinactivation of *Staphylococcus aureus* planktonic cultures upon 460 nm irradiation in the presence of (A) GO, Mo<sub>6</sub> or GO/Mo<sub>6</sub> (0.01 g L<sup>-1</sup>) and (B) aged Mo<sub>6</sub> and GO/Mo<sub>6</sub>. Dark controls are represented with black bars and bars labelled Control are experiments in the absence of GO, Mo<sub>6</sub> or GO/Mo<sub>6</sub>.

In the absence of light, GO, Mo<sub>6</sub> and GO/Mo<sub>6</sub> were non-toxic against *S. aureus* at the used concentration of 0.01 mg mL<sup>-1</sup> (Fig. 7A). GO sheets were previously reported to exert an antibacterial effect on *S. aureus*, however in our case we did not observe such effect possibly due to lower concentration and bigger lateral size for the GO used in our experiments.<sup>40</sup> Upon irradiation at 460 nm, GO remained non-toxic, while Mo<sub>6</sub> displayed a mild photoinactivation with a relative decrease of the CFU to  $29 \pm 12\%$  compared to the control, an effect comparable to previous investigations on the antibacterial activity of this complex.<sup>3</sup> Under the same conditions the photoinactivation ability of GO/Mo<sub>6</sub> was remarkable with a relative decrease of the CFU to  $0.06 \pm 0.01\%$  compared to the irradiated control, i. e., the killing was almost three orders of magnitude more efficient than for Mo<sub>6</sub> only (Fig. 7A). Photoinduced intracellular oxidative stress was evaluated by incubating *S. aureus* with 0.01 mg/mL of GO/Mo<sub>6</sub> or its individual components in the presence of DCF-DA as an oxidation probe (Fig. S12 in the Supporting Information). While GO/Mo<sub>6</sub> clearly showed increased photoinduced ROS production, when compared to pure GO, the oxidative ability of Mo<sub>6</sub> alone was higher than that of GO/Mo<sub>6</sub>. Possibly, this feature which is in contradiction with the photoinactivation experiments, arises from different subcellular localization of the materials. Indeed, DCF-DA and Mo<sub>6</sub> should be internalized while GO/Mo<sub>6</sub> should be located at the surface of the bacteria as previously described for GO.<sup>13</sup> Aging of the DMSO solutions of Mo<sub>6</sub> for 6 months led to a total loss of the photoinactivation ability due to hydrolysis of the complex evidently triggered by water traces in DMSO, as previously reported for this complex.<sup>3</sup> On the other hand, aged GO/Mo<sub>6</sub> nanocomposites maintained a high photoinactivation efficiency with a CFU of  $0.37 \pm$

0.26 % (Fig. 7B). The robustness of the system that allows for long-term storage in DMSO suggests a protective of the GO sheets against the hydrolysis of the clusters. Overall, the observed enhancement of the efficiency of the photoinactivation of *S. aureus* was clearly related to a synergistic effect of both components, GO and Mo<sub>6</sub>, probably originating from photoinduced electron transfer from the triplet states of excited Mo<sub>6</sub> to GO leading to the formation of reactive oxygen species.

## Experimental

*Reagents and general procedures.* Compound [ $\{\text{Mo}_6\text{I}_8\}(\text{OCOC}_4\text{H}_8\text{PPh}_3)_6\text{]Br}_4$  (Mo<sub>6</sub>) was prepared according to a previously published procedure.<sup>3</sup> Molybdenum, iodine, sodium methanolate and (4-carboxybutyl)triphenylphosphonium bromide were obtained from Sigma Aldrich and used as received. Solvents for synthesis were purchased from Penta (Czech Republic) and dried over molecular sieves (3 Å). The following reagents were used for the synthesis of graphene oxide without purification: graphite powder (Wako, 98.0%), sulfuric acid (Wako, 95%), sodium nitrate (Wako, 98.0%), potassium permanganate (Kanto, 99.3%), hydrogen peroxide (Kanto, 30.0%), hydrochloric acid (Wako, 35.0%-37.0%).

Raman measurements were recorded with an in Via Reflex spectrometer operating at 732 nm. X-ray photoelectron spectroscopy (XPS) measurements were performed with a JEOL JPS-9010TR spectrometer. Atomic force microscope (AFM) images were obtained using the AFM multimode function on a Digital Instruments AFM. Images of the nanoparticles were acquired by a JEOL 2100 transmission electron microscope (JEOL, Japan). Size distributions and corresponding zeta potentials were determined by dynamic light scattering (DLS) on a particle size analyzer Zetasizer Nano ZS (Malvern, UK). Powder X-ray diffraction (XRD) patterns were recorded using a PANalytical X'Pert PRO diffractometer in the transmission setup equipped with a conventional Cu X-ray tube (40 kV, 30 mA). The molybdenum content of GO/Mo<sub>6</sub> was measured by inductively coupled plasma mass spectrometry (ICP-MS, PerkinElmer, Concord, ON, Canada). The sample was isolated by centrifugation of the GO/Mo<sub>6</sub> water dispersion (10 000 rpm, 5 min), and drying of the solid under reduced pressure for 24 hours. Quantification was carried out via external calibration. The ICP-MS measurement conditions were as follows: RF power 1.1 kW, nebulizer gas flow rate 0.76 L min<sup>-1</sup>, auxiliary gas flow rate 1 L min<sup>-1</sup>, plasma gas flow rate 11 L min<sup>-1</sup>, measured isotope <sup>98</sup>Mo as an analyte and <sup>115</sup>In as an internal standard. UV-vis absorption spectra and luminescence properties were measured on an FLS1000 spectrometer (Edinburgh Instruments, UK) using a cooled PMT-900 photon detection module (Edinburgh Instruments, UK). Aqueous dispersions (0.1 mg mL<sup>-1</sup>

1  
2  
3 GO/Mo<sub>6</sub>) were saturated with air or argon to assure different oxygen concentrations for  
4 phosphorescence analyses. The FLS1000 spectrometer was also used for time-resolved  
5 phosphorescence measurements ( $\lambda_{\text{exc}} = 405 \text{ nm}$ , VPLED Series) and the recorded decay curves  
6 were fitted to exponential functions by the Fluoracle software (v. 2.13.2, Edinburgh  
7 Instruments, UK). Phosphorescence quantum yields of the samples were recorded using a  
8 Quantaury QY C11347-1 spectrometer (Hamamatsu, Japan). Singlet oxygen phosphorescence  
9 was measured on a Fluorolog 3 spectrometer using a Hamamatsu H10330-45 photomultiplier.  
10 In this case, aqueous dispersions of similar absorbance were saturated with oxygen to magnify  
11 phosphorescence signals of O<sub>2</sub>(<sup>1</sup> $\Delta_g$ ). Evaluation of the photoinduced oxidation of DCF-DA was  
12 performed by adding 10  $\mu\text{M}$  of DCF-DA to the GO/Mo<sub>6</sub> water dispersion (0.01  $\text{mg mL}^{-1}$ ),  
13 illuminating with a 12x10 W LED source (Cameo) (460 nm, 18  $\text{mW cm}^{-2}$ ) for 0, 2, 4, and 6  
14 min and measuring the fluorescence of the whole suspension at 488/525 nm.

15  
16  
17  
18  
19  
20  
21  
22  
23  
24 *Preparation of graphene oxide.* Graphene oxide (GO) was synthesized based on the Hummer's  
25 method. Sulfuric acid (92 mL), sodium nitrate (2 g) and graphite (2 g) were added to a 500 mL  
26 beaker and stirred for 30 minutes in an ice bath. After adding potassium permanganate (10 g),  
27 the mixture was stirred at 35°C for 40 min. After adding pure water (92 mL) again in the ice  
28 bath, the mixture was stirred at 70°C for 20 min. Then, pure water (200 mL) was added, and  
29 30% hydrogen peroxide was added little by little until the absence of formation of bubbles. The  
30 precipitate obtained by centrifugation (3000 rpm, 10 min) was washed with 5% hydrochloric  
31 acid and pure water. Centrifugation (15000 rpm, 40 min) was performed to remove ions such  
32 as sulphate ions that cause a decrease in pH, and the supernatant was discarded. The obtained  
33 precipitate was dispersed in pure water and centrifuged to collect the supernatant (8000 rpm,  
34 30 min). Finally, the GO dispersion was concentrated by centrifugation (15000 rpm, 40 min)  
35 to reach a concentration of 1  $\text{g L}^{-1}$ .

36  
37  
38  
39  
40  
41  
42  
43  
44  
45 *Preparation of GO/Mo<sub>6</sub> dispersions.* The colloidal dispersions of GO were freeze dried to  
46 collect dehydrated GO. The freeze-drying method prevents any restacking of the sheets and  
47 facilitates their dispersion in other solvents. Then, colloidal dispersions of GO in DMSO were  
48 prepared at a concentration of 1  $\text{g L}^{-1}$ . [ $\{\text{Mo}_6\text{I}_8\}(\text{OCOC}_4\text{H}_8\text{PPh}_3)_6\text{Br}_4$ , dissolved in DMSO  
49 solvent at a concentration of 1  $\text{g L}^{-1}$ , was added to the GO dispersions. The resulting dispersions  
50 were stirred at 200 rpm for 1 day and directly used for formation of water dispersions  
51 (DMSO:H<sub>2</sub>O v:v=0.01).

52  
53  
54  
55  
56  
57 *Photoinactivation of bacteria and ROS determination.* Bacterial samples of *Staphylococcus*  
58 *aureus* were cultivated at 37 °C and stored at 4 °C either in the liquid Luria-Bertani (LB)  
59  
60

1  
2  
3 medium or on LB agar. The stock solutions of Mo<sub>6</sub> were prepared in DMSO. All experiments  
4 were performed in triplicates. The stock inoculum of *Staphylococcus aureus* was prepared by  
5 diluting bacteria in water and standardizing suspension to 1 McF. A 100 μL aliquot of the  
6 inoculum was taken and mixed with GO, Mo<sub>6</sub> or GO/Mo<sub>6</sub> to a final concentration of 0.01 mg  
7 mL<sup>-1</sup>. The samples were incubated for 2 h in the dark at laboratory temperature and afterwards  
8 irradiated with a 12x10 W LED source (Cameo) (460 nm, 18 mW cm<sup>-2</sup>, 15 min). For  
9 quantification of inactivated bacteria, the Miles and Misra method on LB agar was used.  
10 Evaluation of the photoinduced oxidation of DCF-DA was performed by treating inoculum of  
11 *S. aureus* at 1 McF in water with 0.01 mg mL<sup>-1</sup> of GO, Mo<sub>6</sub> or GO/Mo<sub>6</sub> (1% DMSO) for 2  
12 hours, adding DCF-DA in DMSO to a final concentration 10 μM, illuminating with with a  
13 12x10 W LED source (Cameo) (460 nm, 18 mW cm<sup>-2</sup>) for 0, 5, and 10 min and measuring the  
14 fluorescence of the whole suspension at 488/525 nm. The control experiments were performed  
15 using the same concentration of DMSO (1% v/v in final suspension) introduced by the addition  
16 of GO, Mo<sub>6</sub> or GO/Mo<sub>6</sub> in the dark or upon irradiation. The effect of aging of dispersions on  
17 the antibacterial activity was performed using 6 months-old DMSO dispersions of Mo<sub>6</sub> and  
18 GO/Mo<sub>6</sub>.

## 31 32 **Conclusion**

33 We have designed a nanocomposite material based on graphene oxide sheets and a Mo<sub>6</sub>  
34 compound. Lyophilization of the GO sheets after preparation allowed for the formation of  
35 stable colloidal dispersions of GO. Upon the addition of the DMSO colloidal dispersions of  
36 GO and Mo<sub>6</sub> to water, the formation of positively charged nanoaggregates of Mo<sub>6</sub> occurred,  
37 followed by their immobilization on the surface of the GO sheets *via* electrostatic interaction  
38 as demonstrated by DLS, TEM, ICP-MS, and absorption and luminescence spectroscopy. In  
39 agreement with electronic properties of GO when combined with photoactive sensitizers,  
40 photoinduced electron transfer from excited states of Mo<sub>6</sub> to GO was suggested for explaining  
41 the dramatic quenching of the triplet states when Mo<sub>6</sub> is associated with GO. This phenomenon  
42 also led to the inhibition of singlet oxygen formation by Mo<sub>6</sub>. Injection of electrons from Mo<sub>6</sub>  
43 into the conduction band of GO led to the formation of reactive oxygen species, possibly  
44 superoxide, hydrogen peroxide or hydroxyl radicals, providing a robust antibacterial activity  
45 against *S. aureus* far stronger than that of the isolated components of the nanocomposite. The  
46 observation of the synergistic effect paves the way for the design of nanomaterials with  
47 enhanced photooxidative properties which potential applications in life and environmental  
48 sciences. The easy preparation of the described material as well as the use of inexpensive  
49  
50  
51  
52  
53  
54  
55  
56  
57  
58  
59  
60

1  
2  
3 components suggest relevant potential for scaling up the production of this nanocomposite  
4 material. From a prospective point of view, we believe that the properties of such  
5 nanocomposite can be further tuned and optimized by the careful choice of apical ligands of  
6 cluster complex and by varying the size, oxidation rate or chemically modifying the surface of  
7 the GO sheets. Also, incorporation of the nanocomposite into functional materials such as  
8 surfaces and membranes could expand the potential for antibacterial and environmental  
9 applications.  
10  
11  
12  
13  
14  
15  
16

### 17 **Supporting Information**

18 Photographs of GO dispersions, TEM and AFM of GO, DLS of Mo<sub>6</sub>, Zeta potentials of GO,  
19 Mo<sub>6</sub> and GO/Mo<sub>6</sub>, powder XRD of GO/Mo<sub>6</sub>, absorption spectra, luminescence spectra,  
20 luminescence decay kinetics, and photoinduced ROS production of GO, Mo<sub>6</sub> and GO/Mo<sub>6</sub>  
21 (.PDF).  
22  
23  
24  
25  
26

### 27 **Acknowledgments**

28 This research work was supported by the Czech Science Foundation (21-16084J) and the Japan  
29 Society for Promotion of Science Kakenhi C project (20K03887). We acknowledge the  
30 assistance provided by the Research Infrastructure NanoEnviCz, supported by the Ministry of  
31 Education, Youth and Sports of the Czech Republic under Project LM2018124. We are grateful  
32 to Petr Bezdička for the measurement of powder XRD pattern and to Antonin Kaňa for the  
33 analysis of the molybdenum content by ICP-MS.  
34  
35  
36  
37  
38  
39  
40  
41  
42  
43  
44  
45  
46  
47  
48  
49  
50  
51  
52  
53  
54  
55  
56  
57  
58  
59  
60

## References

- 1 O'Gara, J. P. Into the storm: Chasing the opportunistic pathogen *Staphylococcus aureus* from skin colonisation to life-threatening infections. *Environmental Microbiology* 2017, 19 (10), 3823-3833, DOI: <https://doi.org/10.1111/1462-2920.13833>.
- 2 Schito, G. C. The importance of the development of antibiotic resistance in *Staphylococcus aureus*. *Clinical Microbiology and Infection* 2006, 12, 3-8, DOI: 10.1111/j.1469-0691.2006.01343.x.
- 3 Kirakci, K.; Zelenka, J.; Rumlová, M.; Cvačka, J.; Ruml, T.; Lang, K. Cationic octahedral molybdenum cluster complexes functionalized with mitochondria-targeting ligands: photodynamic anticancer and antibacterial activities. *Biomaterials Science* 2019, 7 (4), 1386-1392, DOI: 10.1039/C8BM01564C.
- 4 Kirakci, K.; Kubáňová, M.; Příbyl, T.; Rumlová, M.; Zelenka, J.; Ruml, T.; Lang, K. A Cell Membrane Targeting Molybdenum-Iodine Nanocluster: Rational Ligand Design toward Enhanced Photodynamic Activity. *Inorganic Chemistry* 2022, 61 (12), 5076-5083, DOI: 10.1021/acs.inorgchem.2c00040.
- 5 Beltrán, A.; Mikhailov, M.; Sokolov, M. N.; Pérez-Laguna, V.; Rezusta, A.; Revillo, M. J.; Galindo, F. A photobleaching resistant polymer supported hexanuclear molybdenum iodide cluster for photocatalytic oxygenations and photodynamic inactivation of *Staphylococcus aureus*. *Journal of Materials Chemistry B* 2016, 4 (36), 5975-5979, DOI: 10.1039/C6TB01966H.
- 6 Felip-León, C.; Arnau del Valle, C.; Pérez-Laguna, V.; Isabel Millán-Lou, M.; Miravet, J. F.; Mikhailov, M.; Sokolov, M. N.; Rezusta-López, A.; Galindo, F. Superior performance of macroporous over gel type polystyrene as a support for the development of photo-bactericidal materials. *Journal of Materials Chemistry B* 2017, 5 (30), 6058-6064, DOI: 10.1039/C7TB01478C.
- 7 Kirakci, K.; Nguyen, T. K. N.; Grasset, F.; Uchikoshi, T.; Zelenka, J.; Kubát, P.; Ruml, T.; Lang, K. Electrophoretically Deposited Layers of Octahedral Molybdenum Cluster Complexes: A Promising Coating for Mitigation of Pathogenic Bacterial Biofilms under Blue Light. *ACS Applied Materials & Interfaces* 2020, 12 (47), 52492-52499, DOI: 10.1021/acsami.0c19036.
- 8 Vorotnikova, N. A.; Alekseev, A. Y.; Vorotnikov, Y. A.; Evtushok, D. V.; Molard, Y.; Amela-Cortes, M.; Cordier, S.; Smolentsev, A. I.; Burton, C. G.; Kozhin, P. M.; Zhu, P.; Topham, P. D.; Mironov, Y. V.; Bradley, M.; Efremova, O. A.; Shestopalov, M. A. Octahedral molybdenum cluster as a photoactive antimicrobial additive to a fluoroplastic. *Materials Science and Engineering: C* 2019, 105, 110150, DOI: <https://doi.org/10.1016/j.msec.2019.110150>.
- 9 Ngan T. K. Nguyen, Clément Lebastard, Maxence Wilmet, Noée Dumait, Adèle Renaud, Stéphane Cordier, Naoki Ohashi, Tetsuo Uchikoshi & Fabien Grasset (2022) A review on functional nanoarchitectonics nanocomposites based on octahedral metal atom clusters (Nb<sub>6</sub>, Mo<sub>6</sub>, Ta<sub>6</sub>, W<sub>6</sub>, Re<sub>6</sub>): inorganic 0D and 2D powders and films, *Science and Technology of Advanced Materials*, 23:1, 547-578, DOI: 10.1080/14686996.2022.2119101
- 10 Maverick, A. W.; Najdzionek, J. S.; MacKenzie, D.; Nocera, D. G.; Gray, H. B. Spectroscopic, electrochemical, and photochemical properties of molybdenum(II) and tungsten(II) halide clusters. *Journal of the American Chemical Society* 1983, 105 (7), 1878-1882, DOI: 10.1021/ja00345a034.
- 11 Kirakci, K.; Kubát, P.; Dušek, M.; Fejfarová, K.; Šícha, V.; Mosinger, J.; Lang, K. A Highly Luminescent Hexanuclear Molybdenum Cluster – A Promising Candidate toward Photoactive Materials. *European Journal of Inorganic Chemistry* 2012, 2012 (19), 3107-3111, DOI: <https://doi.org/10.1002/ejic.201200402>.
- 12 Kirakci, K.; Kubát, P.; Langmaier, J.; Polívka, T.; Fuciman, M.; Fejfarová, K.; Lang, K. A comparative study of the redox and excited state properties of (nBu<sub>4</sub>N)<sub>2</sub>[Mo<sub>6</sub>X<sub>14</sub>] and

(nBu<sub>4</sub>N)<sub>2</sub>[Mo<sub>6</sub>X<sub>8</sub>(CF<sub>3</sub>COO)<sub>6</sub>] (X = Cl, Br, or I). Dalton Transactions 2013, 42 (19), 7224-7232, DOI: 10.1039/C3DT32863E.

13 Liu, S.; Zeng, T. H.; Hofmann, M.; Burcombe, E.; Wei, J.; Jiang, R.; Kong, J.; Chen, Y. Antibacterial Activity of Graphite, Graphite Oxide, Graphene Oxide, and Reduced Graphene Oxide: Membrane and Oxidative Stress. ACS Nano 2011, 5 (9), 6971-6980, DOI: 10.1021/nn202451x.

14 McCoy, T. M.; Turpin, G.; Teo, B. M.; Tabor, R. F. Graphene oxide: a surfactant or particle? Current Opinion in Colloid & Interface Science 2019, 39, 98-109, DOI: <https://doi.org/10.1016/j.cocis.2019.01.010>.

15 Zhao, Y.; Hsieh, H.-S.; Wang, M.; Jafvert, C. T. Light-independent redox reactions of graphene oxide in water: Electron transfer from NADH through graphene oxide to molecular oxygen, producing reactive oxygen species. Carbon 2017, 123, 216-222, DOI: <https://doi.org/10.1016/j.carbon.2017.07.048>.

16 Guo, Z.; Zhang, P.; Xie, C.; Voyiatzis, E.; Faserl, K.; Chetwynd, A. J.; Monikh, F. A.; Melagraki, G.; Zhang, Z.; Peijnenburg, W. J. G. M.; Afantitis, A.; Chen, C.; Lynch, I. Defining the Surface Oxygen Threshold That Switches the Interaction Mode of Graphene Oxide with Bacteria. ACS Nano, 2023, 17, 6350–6361. <https://doi.org/10.1021/acsnano.2c10961>.

17 Yadav, S.; Singh Raman, A. P.; Meena, H.; Goswami, A. G.; Bhawna; Kumar, V.; Jain, P.; Kumar, G.; Sagar, M.; Rana, D. K.; Bahadur, I.; Singh, P. An Update on Graphene Oxide: Applications and Toxicity. ACS Omega, 2022, 7, 35387–35445. <https://doi.org/10.1021/acsomega.2c03171>.

18 Chen, C.; Yu, W.; Liu, T.; Cao, S.; Tsang, Y. Graphene oxide/WS<sub>2</sub>/Mg-doped ZnO nanocomposites for solar-light catalytic and anti-bacterial applications. Solar Energy Materials and Solar Cells 2017, 160, 43-53, DOI: <https://doi.org/10.1016/j.solmat.2016.10.020>.

19 Gayathri, S.; Jayabal, P.; Kottaisamy, M.; Ramakrishnan, V. Synthesis of ZnO decorated graphene nanocomposite for enhanced photocatalytic properties. Journal of Applied Physics 2014, 115 (17), 173504, DOI: 10.1063/1.4874877.

20 Tao, Y.; Lin, Y.; Huang, Z.; Ren, J.; Qu, X. Incorporating graphene oxide and gold nanoclusters: a synergistic catalyst with surprisingly high peroxidase-like activity over a broad pH range and its application for cancer cell detection. Adv Mater 2013, 25 (18), 2594-2599, DOI: 10.1002/adma.201204419.

21 Wang, B.; Moon, J. R.; Ryu, S.; Park, K. D.; Kim, J.-H. Antibacterial 3D graphene composite gel with polyaspartamide and tannic acid containing in situ generated Ag nanoparticle. Polymer Composites 2020, 41 (7), 2578-2587, DOI: <https://doi.org/10.1002/pc.25556>.

22 Wang, Y.-W.; Cao, A.; Jiang, Y.; Zhang, X.; Liu, J.-H.; Liu, Y.; Wang, H. Superior Antibacterial Activity of Zinc Oxide/Graphene Oxide Composites Originating from High Zinc Concentration Localized around Bacteria. ACS Applied Materials & Interfaces 2014, 6 (4), 2791-2798, DOI: 10.1021/am4053317.

23 Zhou, L.; Jiang, H.; Wei, S.; Ge, X.; Zhou, J.; Shen, J. High-efficiency loading of hypocrellin B on graphene oxide for photodynamic therapy. Carbon 2012, 50 (15), 5594-5604, DOI: <https://doi.org/10.1016/j.carbon.2012.08.013>.

24 Monteiro, A. R.; Neves, M. G. P. M. S.; Trindade, T. Functionalization of Graphene Oxide with Porphyrins: Synthetic Routes and Biological Applications. ChemPlusChem 2020, 85 (8), 1857-1880, DOI: <https://doi.org/10.1002/cplu.202000455>.

25 Feliz, M.; Atienzar, P.; Amela-Cortés, M.; Dumait, N.; Lemoine, P.; Molard, Y.; Cordier, S. Supramolecular Anchoring of Octahedral Molybdenum Clusters onto Graphene and Their Synergies in

Photocatalytic Water Reduction. *Inorg. Chem.* 2019, 58, 15443–15454. <https://doi.org/10.1021/acs.inorgchem.9b02529>.

26 Puche, M.; García-Aboal, R.; Mikhaylov, M. A.; Sokolov, M. N.; Atienzar, P.; Feliz, M. Enhanced Photocatalytic Activity and Stability in Hydrogen Evolution of Mo<sub>6</sub> Iodide Clusters Supported on Graphene Oxide. *Nanomater.*, 2020, 10, 1259. <https://doi.org/10.3390/nano10071259>.

27 Casanova-Chafer, J.; Garcia-Aboal, R.; Atienzar, P.; Feliz, M.; Llobet, E. Octahedral Molybdenum Iodide Clusters Supported on Graphene for Resistive and Optical Gas Sensing. *ACS Appl. Mater. Interfaces*, 2022, 14, 57122–57132. <https://doi.org/10.1021/acsami.2c15716>.

28 Barras, A.; Das, M. R.; Devarapalli, R. R.; Shelke, M. V.; Cordier, S.; Szunerits, S.; Boukherroub, R. One-Pot Synthesis of Gold Nanoparticle/Molybdenum Cluster/Graphene Oxide Nanocomposite and Its Photocatalytic Activity. *Applied Catalysis B: Environmental*, 2013, 130–131, 270–276. <https://doi.org/10.1016/j.apcatb.2012.11.017>.

29 Feliz, M.; Puche, M.; Atienzar, P.; Concepción, P.; Cordier, S.; Molard, Y. In Situ Generation of Active Molybdenum Octahedral Clusters for Photocatalytic Hydrogen Production from Water. *ChemSusChem*, 2016, 9, 1963–1971. <https://doi.org/10.1002/cssc.201600381>.

30 Hummers, W. S.; Offeman, R. E. Preparation of Graphitic Oxide. *J. Am. Chem. Soc.* 1958, 80, 1339. <https://doi.org/10.1021/ja01539a017>.

31 Paredes, J. I.; Villar-Rodil, S.; Martínez-Alonso, A.; Tascón, J. M. D. Graphene Oxide Dispersions in Organic Solvents. *Langmuir* 2008, 24 (19), 10560–10564, DOI: 10.1021/la801744a.

32 Priante, F.; Salim, M.; Ottaviano, L.; Perrozzi, F. XPS study of graphene oxide reduction induced by (100) and (111)-oriented Si substrates. *Nanotechnology* 2018, 29 (7), 075704, DOI: 10.1088/1361-6528/aaa320.

33 Kirakci, K.; Zelenka, J.; Rumlová, M.; Martinčík, J.; Nikl, M.; Ruml, T.; Lang, K. Octahedral Molybdenum Clusters as Radiosensitizers for X-Ray Induced Photodynamic Therapy. *Journal of Materials Chemistry B*, 2018, 6, 4301–4307. <https://doi.org/10.1039/c8tb00893k>.

34 Sciortino, F.; Cuny, J.; Grasset, F.; Lagrost, C.; Lemoine, P.; Moréac, A.; Molard, Y.; Takei, T.; Cordier, S.; Chevance, S.; Gauffre, F. The Ouzo Effect to Selectively Assemble Molybdenum Clusters into Nanomarbles or Nanocapsules with Increased HER Activity. *Chemical Communications*, 2018, 54, 13387–13390. <https://doi.org/10.1039/c8cc07402j>.

35 Koncošová, M.; Rumlová, M.; Mikyšková, R.; Reiniš, M.; Zelenka, J.; Ruml, T.; Kirakci, K.; Lang, K. Avenue to X-Ray-Induced Photodynamic Therapy of Prostatic Carcinoma with Octahedral Molybdenum Cluster Nanoparticles. *Journal of Materials Chemistry B*, 2022, 10, 3303–3310. <https://doi.org/10.1039/d2tb00141a>.

36 Felip-León, C.; Puche, M.; Miravet, J. F.; Galindo, F.; Feliz, M. A Spectroscopic Study to Assess the Photogeneration of Singlet Oxygen by Graphene Oxide. *Materials Letters*, 2019, 251, 45–51. <https://doi.org/10.1016/j.matlet.2019.05.001>.

37 Panda, S.; Rout, T. K.; Prusty, A. D.; Ajayan, P. M.; Nayak, S. Electron Transfer Directed Antibacterial Properties of Graphene Oxide on Metals. *Advanced Materials*, 2018, 30, 1702149. <https://doi.org/10.1002/adma.201702149>.

38 Chong, Y.; Ge, C.; Fang, G.; Wu, R.; Zhang, H.; Chai, Z.; Chen, C.; Yin, J.-J. Light-Enhanced Antibacterial Activity of Graphene Oxide, Mainly via Accelerated Electron Transfer. *Environmental Science & Technology*, 2017, 51, 10154–10161. <https://doi.org/10.1021/acs.est.7b00663>.

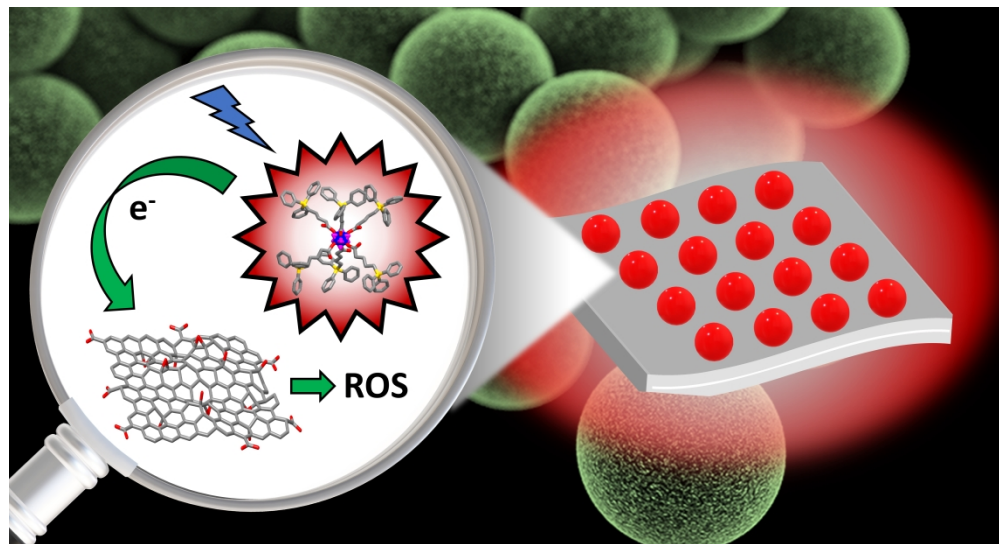
39 Vinoth, R.; Babu, S. G.; Bharti, V.; Gupta, V.; Navaneethan, M.; Bhat, S. V.; Muthamizhchelvan, C.; Ramamurthy, P. C.; Sharma, C.; Aswal, D. K.; Hayakawa, Y.; Neppolian, B. Ruthenium Based

1  
2  
3  
4  
5  
6  
7  
8  
9  
10  
11  
12  
13  
14  
15  
16  
17  
18  
19  
20  
21  
22  
23  
24  
25  
26  
27  
28  
29  
30  
31  
32  
33  
34  
35  
36  
37  
38  
39  
40  
41  
42  
43  
44  
45  
46  
47  
48  
49  
50  
51  
52  
53  
54  
55  
56  
57  
58  
59  
60

---

Metallopolymer Grafted Reduced Graphene Oxide as a New Hybrid Solar Light Harvester in Polymer Solar Cells. *Scientific Reports*, 2017, 7. <https://doi.org/10.1038/srep43133>.

40 Zappacosta, R.; Di Giulio, M.; Ettore, V.; Bosco, D.; Hadad, C.; Siani, G.; Di Bartolomeo, S.; Cataldi, A.; Cellini, L.; Fontana, A. Liposome-Induced Exfoliation of Graphite to Few-Layer Graphene Dispersion with Antibacterial Activity. *Journal of Materials Chemistry B*, 2015, 3, 6520–6527. <https://doi.org/10.1039/c5tb00798d>.



Photoinduced electron transfer in a graphene oxide/molybdenum cluster nanocomposite material leads to enhanced *Staphylococcus aureus* photoinactivation.

329x178mm (600 x 600 DPI)